Modern Research and Educational Topics in Microscopy.
A. Méndez-Vilas and J. Díaz (Eds.)

Atomic Force Microscope Nanoindentations to Reliably Measure the Young's Modulus of Soft Matter

D. Tranchida, Z. Kiflie, and **S. Piccarolo**[*]

Dipartimento di Ingegneria Chimica dei Processi e dei Materiali, Università di Palermo, Viale delle Scienze, 90128 Palermo, Italy and INSTM Udr Palermo

The analysis of nanomechanical properties is becoming an increasingly useful tool in a large variety of fields, ranging from biology to polymer science. The Atomic Force Microscope, AFM, can bridge the information about morphology, obtained with outstanding resolution, to local mechanical properties. When performing an AFM nanoindentation, the rough force curve, i.e. the plot of voltage output from the photodiode vs. the voltage applied to the piezoscanner, can be translated into a curve of the applied load vs. penetration depth after a series of preliminary determinations and calibrations. The Young's modulus of the sample can be finally extracted from the force curve, through a correct application of contact mechanics models. All the calibrations needed are thoroughly described in this work, together with the details about contact mechanics, in order to clarify the correct procedure needed for the analysis of nanomechanical properties through AFM nanoindentations.

Keywords atomic force microscopy; nanoindentation; Young's modulus

1. Introduction

Nanoindentation is a relatively new technique. Normally, nanoindentation tests are carried out using Depth Sensing Instruments, DSI. The Atomic Force Microscope, AFM, can also be used as a DSI, in order to perform nanoindentations and thus measure the Young's modulus on the nanometer scale. When used as a microscope, the AFM tip is scanned laterally on the top of the sample surface while as a DSI the AFM tip is used as an indenter, in which case a force curve would be obtained by recording the applied load on the tip with the corresponding penetration depth. The load on the tip is applied through a bending cantilever, which is not usually stiff enough to indent metals or ceramic materials. For this reason, AFM nanoindentation is mainly useful to measure mechanical properties of soft matter, especially biological materials[1] and polymers.[2] In case of polymers in particular, it is used for the study of the mechanical properties of single phases in non-homogeneous systems as well as for the mapping of the Young's modulus of samples characterized by structural variation thus becoming a powerful tool to bridge structure with properties.

However, rare papers tried to quantitatively measure the Young's modulus of polymers directly from the force curve, i.e., from the plot of applied load vs. penetration depth. The cause of this general but not systematically quantitative use of AFM nanoindentations can be found in the number of calibrations and preliminary determinations needed to apply contact mechanics models to the rough force curve obtained from the nanoindentations, i.e., expressed as the output voltage from the position sensitive diode vs. the voltage applied to the piezoscanner. Several aspects, such as sample thickness and surface roughness, must be considered, and many parameters like cantilever normal elastic constant, deflection sensitivity, relationship between cantilever deflection and applied load, piezo aging, instrument compliance need to be accurately known for this rough force curve to be properly and correctly expressed as force vs. penetration depth.

Although a relatively large amount of literature is available,[3] some aspects of the numerous calibrations needed have not yet been clearly reported and the proper use of the technique is currently hard and not widespread. The procedure commonly followed in our laboratories to analyze the rough

[*] Corresponding author: e-mail: Piccarolo@unipa.it

force curve is addressed in this work, showing the pathway to obtain a reliable evaluation of the Young's modulus of polymers on nanometre scale.

2. Materials used and experimental set-up

The materials studied in this work were chosen to cover a wide range of mechanical properties. These include rubbers (PPG-based), semicrystalline (iPP, HDPE, PTFE) and glassy polymers (PMMA, PC) having elastic moduli in the range 7-3000 MPa.

Poly (methyl methacrylate), PMMA, (M_w=120000) and Poly(propylenglycole), PPG, (M_w=725 and dispersion index 1.04) were purchased from Aldrich. Poly (carbonate), PC, (M_w=39000) and a research grade High Density Poly (ethylene), HDPE, were kindly supplied by DSM. iPP (M_n=75100, M_w=483000, M_w/M_n=6.4) was provided by Montell while a commercial grade PTFE, 50 μm thick film, was used as purchased from Goodfellow.

PMMA and PC samples were prepared by hot stage (Mettler-Toledo FP82HT with FP90 central processor). iPP samples were prepared with four cooling rates (2.5, 25, 110, 350 K/s) corresponding to the onset of the stable crystalline α-monoclinic phase, decreasing in amount with cooling rate, up to 350 K/s where the onset of the metastable mesomorphic phase is observed[4]. PPG based rubber was synthesized by the authors according to literature[5].

The AFM used was a Digital Instrument Nanoscope IIIA Multimode. The polymer morphology was studied in tapping mode at room temperature in the moderate tapping regime[6] ($0.6 < r_{SP} < 0.75$). Tapping silicon cantilevers (model TESP of Digital Instruments Inc. with nominal cantilever elastic constant of 30 N/m; as well as SNS18 and SNS14 of Micromasch with nominal cantilever elastic constant of 40 and 3 N/m respectively) were used. Loads ranged from ca 0.06 μN up to 4 μN.

The Finite Elements Analysis was carried out using solid (for the tip) and shell elements (for the cantilever) in the MARC 6.0 software package.

Scanning Electron Microscope images were collected with a Philips XL30 ESEM.

3. AFM calibrations and instrumental issues

Film thickness limits the scale on which the nanoindentations can be performed, because with too deep indentations the mechanical behaviour would result from the coupled sample and substrate properties[7]. Without going to very accurate analysis (see, e.g., Hsue and Miranda[8] and references therein), a rule of thumb to avoid substrate effects would be to work at penetration depths less than one tenth of the total film thickness, a condition which is more than satisfied by the films used in the present work.

Sample roughness can also introduce distortion in the force curve, the contact developing between sample asperities and the tip. Studies made regarding the influence of roughness on indentation of metals date back to Tabor,[9] while recent works include those made on "roughened polymers".[10] As discussed in the following, this might be related to the onset of torsional momentum, causing a twist of the tip[11]. So, to overcome these limitations, samples with very low local roughness (in the range 1-3 nm on a 1μm by 1μm scale) were prepared.

Cantilever normal elastic constant, k_n, is a quantity that is used to estimate the instantaneous applied load, F, from the experimentally available cantilever deflection, δ, through the following relation:

$$F = k_n \delta \tag{1}$$

Typical deviations of up to ±200%[12] from the nominal value supplied by the producer are possible when thin cantilevers are used. This error will obviously lead to a wrong evaluation of the applied load in the nanoindentation, which means that k_n should be known with good accuracy. Complex and refined methods, such as measuring the static deflection caused by spheres of known mass attached to the cantilever,[13] have been proposed for its calibration. However, most of these methods are hardly suitable for a routine and high-throughput use of AFM nanoindentations.

Polymers are often relatively stiff and thus require the application of loads in the order of a few microNewtons for their nanoindentations. This implies that stiff rectangular tapping cantilever can be used. The simple geometry of these cantilevers introduces less errors in the elastic constant evaluation from the knowledge of cantilever geometry, compared to the questioned parallel beam approximation for the compliant V-shaped cantilevers used for contact imaging.
The method introduced by Green et al.[14], which has previously been proven to be accurate, is used in the present work, see eqs. 2 and 3. It consists of measuring the length, L, and width of the cantilever from an SEM image. The cantilever thickness, t, is then evaluated from:

$$t = \frac{f_r L^2}{0.162}\left[\frac{\rho}{E}\right]^{1/2} \tag{2}$$

Where f_r, ρ and E are the cantilever resonance frequency, density and Young's modulus, respectively.
Two exemplar SEM images of the cantilever are shown in Figure 1.

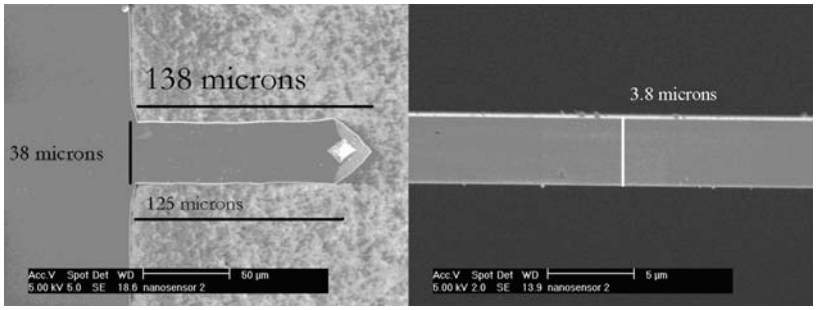

Fig. 1 SEM images of a representative cantilever, used to measure its length, width and thickness as indicated

The first two entries of Table 1 compare the length and width provided by the manufacturer with those read from the image in Figure 1A. It can be seen that the differences are noticeable and this turns out to be very important since cantilever thickness is calculated based on these two values in addition to the cantilever resonance frequency. In fact, the table also shows the calculated thickness of 3.2 and 3.9 μm respectively obtained using the manufacturer data and length read from SEM. Furthermore, respectively comparing these calculated values with the true cantilever thickness (3.8 μm, see Figure 1B), error values of 15% and 2.5% are obtained showing a good agreement for the latter case, the small error being probably due to the non-rectangular cantilever shape at the apex.

Table 1 Comparison of length and width as provided by the manufacturer and as measured from SEM images. The corresponding evaluated thicknesses and respective errors are also indicated.

Length, μm	125 (1)	138 (2)
Width, μm	30 (1)	38 (2)
Evaluated thickness, μm	3.2	3.9
Error*	15%	2.5%

(1) from producer; (2) from SEM images of the cantilever
* error of the evaluated thickness with respect to the thickness measured through SEM images

The cantilever normal elastic constant obtained from theoretical models has also been compared to that from numerical simulations. However, as it can be observed in Figure 1A, the cantilever shape is not exactly rectangular, but rather trapezoidal. This feature has been properly taken into account for further numerical simulations, as shown in Figure 2 where the cantilever shape used for simulation is depicted, thus trying to keep it as close as possible to the real shape observed in SEM, together with the mesh used.

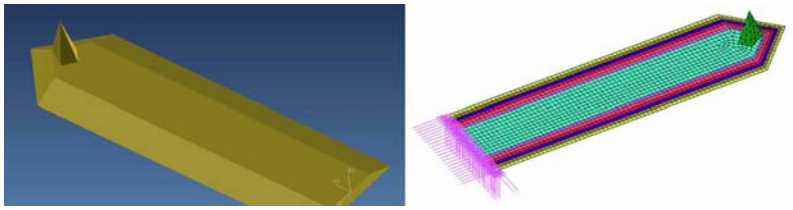

Fig. 2 Finite Element Simulation of the AFM cantilever. On the left, the bare geometry is depicted while the mesh used is shown on the right

The simulated elastic constant (as obtained by numerical analysis) was compared to the one estimated from the theoretical solution of the mechanical problem consisting in a trapezoidal section cantilever bending under load. In this latter case, the normal cantilever elastic constant is evaluated through:

$$k_n = \frac{3EI_G}{L^3} \tag{3}$$

Where I_G is the momentum of inertia for the cantilever section, including, among other quantities, also the cantilever width.

Considering the real trapezoidal cantilever section, a problem arises for numerical simulations, since solid elements used to model the bent sides of the cantilever are less accurate. A slightly different section is therefore needed, as a step-wise border, named "simplified section" in Table 2. In this case, the mismatch between the analytical and the numerical solutions is fairly severe, amounting to 15%. Therefore, a further test was attempted to check whether this error is due to the simplification used in the numerical simulations or to other problems connected with theoretical modelling. The cantilever section was then assumed to be rectangular, allowing in this case a good accuracy for numerical simulations. The agreement between analytical and numerical results in this case is perfect, with an error of only 0.4%. One can then safely infer that the accuracy of the theoretical solution, even for the complex trapezoidal section, is more than satisfactory.

Table 2 Comparison between the elastic constant evaluated by Finite Element Analysis and the one evaluated from the theoretical problem for two different geometries.

	Analytical [N/m]	FEM simulation [N/m]	Error
Elastic constant – Rectangular section	52.7	52.5	0.4%
Elastic constant – Simplified section	37.7	32.1	15%

The linear relationship between cantilever deflection and applied load (eq. 1) was also checked by means of numerical simulations and the results, although not shown here, indicate that the relationship is very accurate up to cantilever deflections of 140 nm.

A further remark concerns the cantilever torsion[11]. Indeed, the cantilever may twist during indentation even if perpendicular loading is preserved by instrumental settings. This happens, especially at the start of the indentation, because of torque arising from the not perfectly vertical loading of the tip due to sample roughness. The torsional elastic constant (k_t) can be calculated by the formula[12]:

$$k_t = k_n \frac{2L^2}{3(1-\nu)} \tag{4}$$

where ν is cantilever Poisson ratio. The equation predicts a torsional constant in the order of $2.40 \cdot 10^{-7}$ Nm/rad assuming typical normal elastic constant of 30 N/m and cantilever length in the order of 125 μm. The typical order of magnitude for loads applied during nanoindentations is in the order of 1 μN. The torque applied on the tip can then be estimated to be 10^{-11} Nm assuming a typical value of 10 μm for the

tip height. Finally, the twist of the cantilever can be estimated, from the ratio of the torque and k_t, to be in the order of 0.024 deg. Since this value is very small, the phenomenon has been neglected.

The lateral displacements have been disregarded as well because the lateral elastic constant is usually several orders of magnitude higher than the normal one[12], producing negligible lateral displacements. Because the motion of the piezo in the z-direction and the cantilever deflection are quite small compared to the total ranges of motion, the error due to **photodiode non linearity** is small[15] for the motions used during these indentation tests and have been also ignored. Slight **piezo aging** between calibrations is estimated to give errors much smaller than 1 nm[15] and it has been ignored as well.

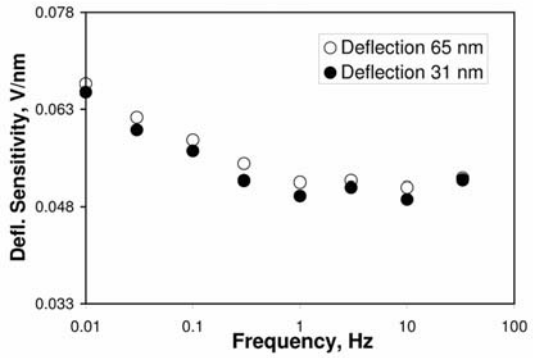

Fig. 3 Deflection sensitivity, obtained from the slope of a force curve performed on a hard material, strongly depends on frequency.

Deflection sensitivity is another important parameter that needs calibration. A rough AFM force curve is a plot of piezo displacement vs. the output voltage from a position sensitive photodiode. The photodiode is used to monitor the cantilever deflection by an optical lever arm system. Therefore, this voltage has to be calibrated so that it can be converted into cantilever deflection. This is done by using a hard material that could not be indented by the tip, so that the cantilever deflection equals the piezo displacement. The deflection sensitivity, D_{sens}, i.e. the conversion factor for translating the voltage into cantilever deflection, will then be obtained from the slope of the plot of the voltage against the piezo displacement. However, the displacement calibration can vary greatly with the set-up and alignment of the cantilever.[11] Due consideration was therefore given to this phenomenon and as such, the deflection sensitivity was calibrated after each set of indentations thus obtaining an accurate calibration regardless of changes in the set-up or laser alignment. Measurement of the deflection sensitivity was also necessary at each tip velocity, because, as shown in Figure 3, the sensitivity changes with the piezo displacement velocity[15] as well as with the amount of cantilever deflection, the changes being considerable at low velocities, while remaining almost constant at higher frequencies.

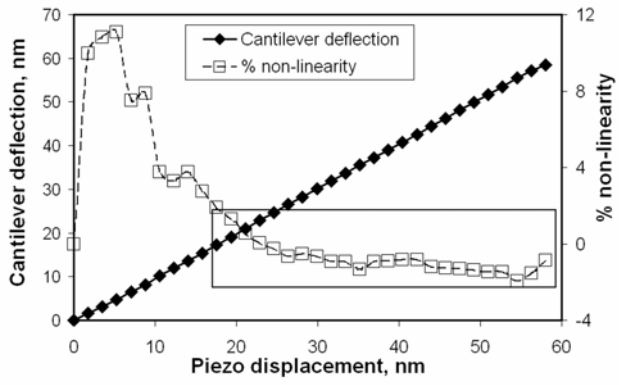

Fig. 4 Deviation of piezo displacement, measured by cantilever deflection on a hard material, from linear dependence on applied voltage.

The non-linearity of piezo displacement can also produce inaccuracy. However, maintaining a constant range of travel was found to yield consistent results for repeated measurements.[15] As shown in Figure 4, the non-linearity, defined as $(z-\delta)/z$, with z being the piezo displacement, is bounded to 2% for piezo

displacements above 20 nm which is acceptable considering that a force curve is usually collected at much higher values of z.

The results are finally corrected for **instrument compliance**, i.e., the cantilever compliance in this case. Assuming no displacement of the material before contact, the penetration depth, *p,* can be obtained from[3]

$$p = z - \delta = z - F / D_{sens} \tag{5}$$

Tip shape was reconstructed by blind estimation, following the theoretical[16] and numerical[17] implementation by Villarrubia and being aware of AFM experimental problems[18]. Tip geometry blind-estimates were performed every time by imaging an aluminium tip-characterizer sample, at a scan frequency of 0.8 Hz and with an image resolution of 512x512 pixel.

A further remark concerns the **loading history** applied during AFM nanoindentation. As it may be obvious, nanoindentation by AFM is done by moving the sample towards the cantilever tip with a constant velocity. Upon contact, indentation starts and the cantilever bends while applying a load. Due to this mechanism, the indentation is neither load controlled nor displacement controlled. Although penetration depth can be obtained using eq. 5, the rate at which this happens cannot be imposed but simply depends on the material.

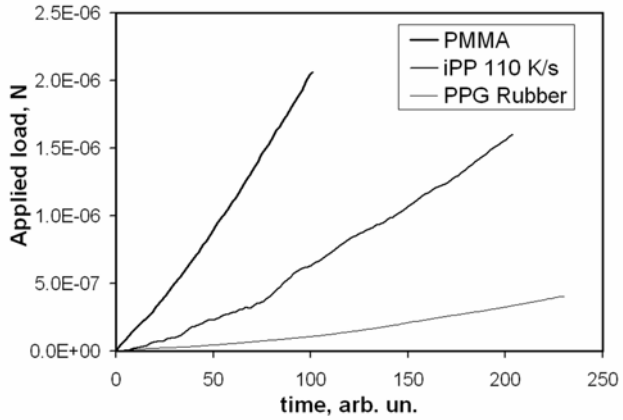

Fig. 5 The complex loading history applied during an AFM nanoindentation depends on material mechanical behavior, see eqs. 6 and 7

The concept that, during AFM nanoindentations, the deformation takes place mostly in the elastic range[2] allows also to rationalize the shape of the curves in Figure 5 where the applied load is plotted against time. Once stated that applied load and penetration depth are related through a power law with exponent 1.5, as it was shown in ref [2], one can notice that cantilever deflection is proportional to applied load through the cantilever elastic constant, eq. 1, and time is proportional to piezo displacement, through the voltage saw tooth applied to the piezo. Thus, recalling also eq. 5,

$$t \propto z \propto (p + \delta) \propto (p + p^{1.5}) \tag{6}$$

And

$$\frac{dt}{dF} \propto \frac{d(p + p^{1.5})}{dF} \propto \frac{dp}{dF} + \frac{dp^{1.5}}{dF} \tag{7}$$

The last term on the right is inversely proportional to the elastic modulus[2] and therefore is a constant (see also the discussion in the following paragraphs). Hence, it is responsible for a linear increase of the load with time. The term *dp/dF* on the other hand is responsible for a non-linear loading history which becomes more relevant if penetration increases more with increasing applied load, i.e. when the material is softer. This could be the explanation why the curve for PMMA in Figure 5 is almost linear while that for PPG rubber shows significant deviations from linearity.

4. Analysis and modelling of contact mechanics

Once the abovementioned calibrations and preliminary determinations are correctly performed, it becomes possible to convert a rough force curve into a plot of applied load vs. penetration depth. The common procedure used to analyze the force curve is the method of Oliver and Pharr[19], which, based on the assumption that the unloading takes place exclusively in the elastic field, uses the results of the elastic analysis of Sneddon. According to Sneddon,[20] the load is supposed to be proportional to the square of the penetration depth, for the case of contact between a cone and an elastic half space. to the square of the penetration depth, for the case of contact between a cone and an elastic half space. Then, the Young's modulus of the sample from nanoindentations is evaluated using the following equation[19]:

$$S = \frac{2}{\sqrt{\pi}} E_r \sqrt{A_c} \tag{8}$$

Where S, contact stiffness, is the derivative of the load with respect to the penetration depth evaluated at maximum load, A_c is the contact area, and E_r is the reduced modulus, i.e., the combination of elastic moduli and Poisson ratio of both the sample and the indenter materials.[19]

Although this approach is widely used for metals and ceramics, limitations to its application on polymers have been recently reported in the case of iPP[21] and PET[22]. As an example, Figure 6 shows the same issue for nanoindentations obtained on a HDPE sample at several cantilever deflections, which are equivalent to applied loads, see eq. 1.

It is easy to note that $\delta \approx z - z_0$ is found on unloading. Here z_0 is a constant and is approximately equal to the value assumed by z during unloading when δ vanishes. Recalling eq. 5, this means that when the load is removed, penetration depth remains almost unaltered so that elastic recovery is very poor and as a result, the slope of the unloading portion of F vs. p curve is very large and, in particular, does not scale with a power law of exponent two. This condition is reported in literature[23] as characteristic of plastic materials. However, this cannot be the case for polymers because, on the contrary, the AFM, allowing one to collect high-resolution images of the residual imprint after the nanoindentation, shows that the plastic depth is in most of the cases much smaller than the penetration depth under full load[2].

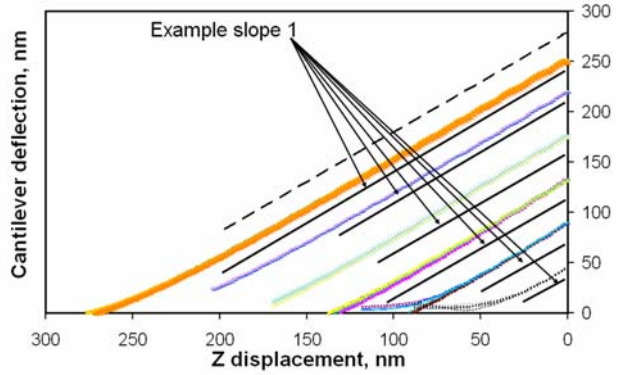

Fig. 6 Unloading nanoindentation curves obtained on a HDPE sample. The slope of the curves is found to be approx. equal to 1.

A different approach is therefore necessary, in order to extract information about the nanometre scale mechanical properties of polymeric samples from AFM nanoindentations.

Performing nanoindentations at different loading rates results in very different sample's mechanical behaviour. In particular, slow nanoindentations leave a relatively large residual imprint on the sample, roughly half of the penetration depth under full load, pointing out the occurrence of complex mechanical phenomena, like viscoelastic, plastic, viscoplastic ones. On the other hand, fast nanoindentations result in small residual indents, up to one fifth of the instantaneous penetration under full load, thus indicating that the mechanical contact for polymers mostly takes place in the elastic range.[2]

Based on this consideration, force curves collected on several materials studied in this work were analyzed by means of Sneddon's purely elastic contact mechanics model.

Unlike the Oliver and Pharr procedure, we did not use the equations for the contact between an ideally sharp cone and an elastic half space. The reason for this choice can be easily found by recalling that a real indenter cannot be considered to be ideally sharp, since rounding is unavoidable on the very first nanometres of the apex because of manufacturing technological constraints.
An alternative uses a dimensional analysis of the indentation quantities[24] involved in a conical indentation of an elastic-plastic material with strain hardening which, for indentations in the nanometer scale, must introduce a length scale for apex rounding. The following dimensionless equation can then be derived:[24]

$$\frac{F}{E_{sample}p^2} = \Pi\left[\frac{l}{p}, \frac{\sigma_Y}{E_{sample}}, \; n, \theta\right] \tag{9}$$

making the exponent, which scales the applied load and the penetration depth, to deviate from two. The strain hardening exponent n, the sample Young's modulus E_{sample}, the yield stress σ_Y, the indenter opening angle θ and the length scale l are the relevant quantities in equation 9. The length scale l can be identified by modelling the tip as a paraboloid of revolution, which, in cylindrical coordinates, is described by

$$\rho^2 = 4qz \tag{10}$$

where q is a constant proportional to the curvature. In this case the length scale is represented by the curvature radius at the apex which, from equation 10, is equal to $2q$.

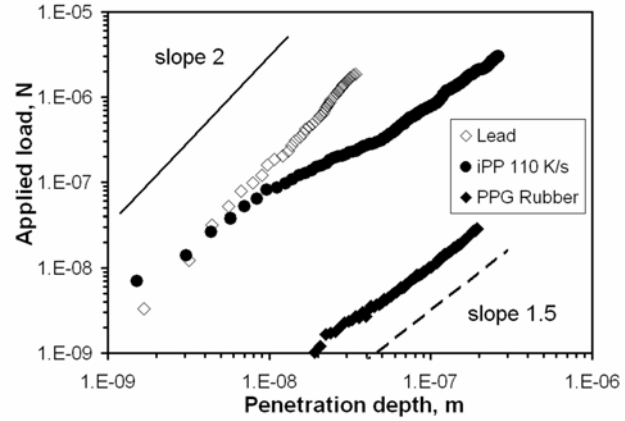

Fig. 7 Logarithmic plot of applied load vs. penetration depth collected on two polymer samples: a PPG rubber and an iPP sample solidified at 110K/s. The typical slope of 1.5 is compared to a metal sample, lead, for which a slope of 2 is measured

The solution for the elastic contact, given by Sneddon[20] satisfies both, the need to introduce a length scale and an exponent smaller than two in

$$F = \frac{4E}{3(1-\nu^2)}\left(2qp^3\right)^{1/2} \tag{11}$$

showing that the load scales with the penetration depth with an exponent of 1.5. Since the Sneddon theory deals with an elastic contact, it adequately describes the force curve in the case of the PPG rubber while it fails to do so for the elastic-plastic material, i.e. lead (see Fig. 7). As expected, the two force curves show different slopes in a logarithmic plot of the penetration depth vs. applied load: almost equal to 1.5 for the PPG rubber and 2 (as predicted for an elastic-plastic contact[25]) for lead. Moreover, the plots are linear, confirming power law relations.
Figure 8 finally shows a comparison among the Young's moduli measured through standard tensile tests, black bars, and the Young's moduli calculated from nanoindentations performed at various piezo displacement rates. It is clear that the evaluated elastic moduli come closer to the macroscopic value with increasing loading rates. However, this result is not surprising since mechanical phenomena other than

elastic becomes negligible at high loading rates,[2] and therefore the assumption of elastic contact in Sneddon's theory is better fulfilled.

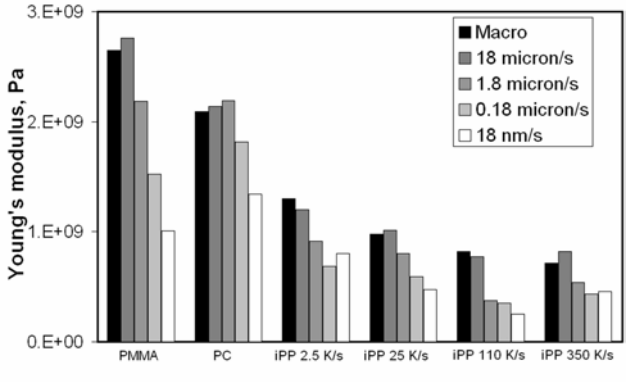

Fig. 8 Comparison of the elastic modulus obtained from AFM nanoindentations by the Sneddon's elastic contact model, with the so called macroscopic one obtained from bulk tensile testing. Here most of the samples tested in this work are reported, covering a very broad range of elastic properties.

A possible criticism arising towards the results shown in Figure 8 is due to the fact that a macroscopic tensile modulus is compared to the one calculated from nanoindentations. In this latter situation, the Young's modulus should likely be closer to the compression modulus rather than the tensile modulus, the former being approx. 20% higher than the latter.[26] In view of the increasing trend of the nanoindentation modulus with the loading rate shown in Figure 8, one might expect that this further gap of 20% could be compensated if nanoindentations were collected at higher loading rates (even higher than 18 μm/s) in order to achieve a completely elastic contact as suggested by the same figure. However under such circumstances nanoindentations performed with piezo-displacement rates higher than 18 μm/s might suffer from instrumental limitations arising form inertia contributions of the piezo scanner upon motion reversal.

However, the trend shown by Figure 8 goes in the right direction and implies that an accurate measurement of the Young's modulus on nanometre scale is possible through AFM nanoindentations. This is confirmed by the comparison with bulk elastic moduli of the samples once their homogeneity is ensured.

This possibility turns out to be very important for a variety of systems, keeping in mind the need for miniaturization in several scientific fields (first of all in semiconductors and thin film applications), but also when a hierarchy of morphologies is present as in the case of most natural materials.

Acknowledgements The authors acknowledge the financial support of the PhD grant of DT by the University of Palermo.

References

[1] D.M. Ebenstein and L.A. Pruitt, NanoToday **1**, 26, (2006)
[2] D. Tranchida, S. Piccarolo, M. Soliman, Macromolecules **39**, 4547 (2006)
[3] B. Cappella and G. Dietler, Surf. Sci. Rep. **34**, 1 (1999)
[4] V. Brucato, S. Piccarolo, V. La Carrubba, Chem. Eng. Sci. **57**, 4129 (2002)
[5] H.H. Bos and J.J.H. Nusselder, Polymer **35**, 2793 (1994)
[6] R. Garcìa and R. Pérez, Surf. Sci. Rep. **47**, 197 (2002)
[7] N.E. Waters, Br. J. Appl. Phys. **16**, 557 (1965)
[8] C.-H. Hsue and P. Miranda, J. Mater. Res. **19**, 94 (2004)
[9] D. Tabor, The Hardness of Metals, Clarendon Press, Oxford (1951)
[10] S.W. Wai, G.M. Spinks, H.R. Brown, M. Swain, Pol. Test. **23**, 501 (2004)
[11] J.R. Pratt, D.T. Smith, D.B. Newell, J. Kramar, E. Whitenton, J. Mater. Res. **19**, 366 (2004)
[12] J.L. Hazel and V.V. Tsukruk, Thin Solid Films **339**, 249 (1999)
[13] T.J.Senden and W.A. Ducker, Langmuir **10**, 1003 (1999)

[14] C.P. Green, H. Lioe, J.P. Cleveland, R. Proksch, P. Mulvaney, J.E. Sader, Rev. Sci. Instr. **75**, 1988 (2004)
[15] M.R. VanLandingham, Micr. Today **97**, 12 (1997)
[16] J.S. Villarrubia, Surf. Sci. **321**, 287 (1994)
[17] J.S. Villarrubia, J. Res. Of NIST **102**, 425 (1997)
[18] D. Tranchida, S. Piccarolo, R.A.C. Deblieck Measuring Science and Technology **17**, 2630 (2006)
[19] W.C. Oliver and G.M. Pharr J.Mater. Res. **7**, 1564 (1992)
[20] I.N. Sneddon, International Journal of Engineering Science **3**, 47 (1965)
[21] D. Tranchida and S. Piccarolo Polymer **46**, 4032 (2005)
[22] D. Tranchida and S. Piccarolo Macromol. Rap. Comm. **26**, 1800 (2005)
[23] J.S. Field and M.V. Swain, J. Mater. Res. **8**, 297 (1993)
[24] Y.-T. Cheng and C.M. Cheng, *Appl. Phys. Lett.* 73, 614 (**1998)**
[25] J. Malzbender, G. de With, J. den Toonder, *J. Mater. Res.* 15 1209 (**2000)**
[26] A. Pawlak and A. Galeski, Macromolecules 38, 9688 (2005)